10-11-2013

# High Field Breakdown Characteristics of Carbon Nanotube Thin Film Transistors

Man Prakash Gupta
*Georgia Institute of Technology*

Ashkan Behnam
*University of Illinois at Urbana-Champaign*

Feifei Lian
*University of Illinois at Urbana-Champaign*

David Estrada
*Boise State University*

Eric Pop
*University of Illinois at Urbana-Champaign*

*See next page for additional authors*

# High Field Characteristics of Carbon Nanotube Thin Film Transistors

**Man Prakash Gupta**
G. W. Woodruff School of Mechanical Engineering
Georgia Institute of Technology
Atlanta, GA 30332, USA

**Ashkan Behnam**
Micro & Nanotechnology Laboratory, and
Dept. of Electrical & Computer Eng.
University of Illinois at Urbana-Champaign
Urbana, IL 61801, USA

**Feifei Lian**
Micro & Nanotechnology Laboratory, and
Dept. of Electrical & Computer Eng.
University of Illinois at Urbana-Champaign
Urbana, IL 61801, USA

**David Estrada**
Micro & Nanotechnology Laboratory, and
Dept. of Electrical & Computer Eng.
University of Illinois at Urbana-Champaign
Urbana, IL 61801, USA

**Eric Pop**
Micro & Nanotechnology Laboratory, and
Dept. of Electrical & Computer Eng.
University of Illinois at Urbana-Champaign
Urbana, IL 61801, USA

and

Beckman Institute for Advanced Science and Technology
University of Illinois at Urbana-Champaign
Urbana, IL 61801, USA

**Satish Kumar**
G. W. Woodruff School of Mechanical Engineering
Georgia Institute of Technology
Atlanta, GA 30332, USA

Email: Satish.kumar@me.gatech.edu

**Abstract**

The high-field properties of carbon nanotube (CNT) network thin film transistors (CN-TFTs) are important for their practical operation, and for understanding their reliability. Using a combination of experimental and computational techniques we show how the channel geometry (length $L_C$ and width $W_C$) and network morphology (average CNT length $L_t$ and alignment angle distribution $\theta$) affect heat dissipation and high-field breakdown in such devices. The results suggest that when $W_C \geq L_t$, the breakdown voltage remains independent of $W_C$ but varies linearly with $L_C$. The breakdown power varies almost linearly with both $W_C$ and $L_C$ when $W_C >> L_t$. We also find that the breakdown power is more susceptible to the variability in the network morphology compared to the breakdown voltage. The analysis offers new insight into the tunable heat dissipation and thermal reliability of CN-TFTs which can be significantly improved through optimization of the network morphology and device geometry.

## 1. Introduction

Carbon nanotubes (CNTs) are promising and useful materials for several applications due to their good thermal, electrical, optical and mechanical properties [1, 2]. Several studies have been performed in the past decade to explore and develop devices which could leverage the excellent properties of individual carbon nanotubes (CNTs) and their two- and three-dimensional (2D and 3D) networks [2-8]. In particular, CNT network thin film transistors (CN-TFTs) have been explored for a wide range of applications such as flexible displays, sensors, antennas, etc. [2, 4, 7-13]. Significant efforts have been made in recent years aimed at overcoming fabrication challenges to improve the performance of these devices [3, 14-19]. However, fewer studies have been focused on the heat dissipation in these devices, which is an important aspect of CN-TFT operation [20, 21]. CNT networks are typically supported on thermally insulating substrates such as glass or plastics, which have very low thermal conductivity and where the excessive self-heating in CN-TFTs under high field operations can lead to the breakdown of these devices [20, 21].

CN-TFTs with a large aspect ratio [(channel length $L_C$ / channel width $W$) $\gg$ 1] have been investigated previously to achieve higher ON/OFF current ratio. Narrow $W_C$ and large $L_C$ in CN-TFTs (Fig. 1) help in reducing the number of metallic percolating paths in unsorted CNT networks which typically have a 1:2 metallic ($M$) – semiconducting ($S$) ratio [3, 22]. However, such high aspect ratios can also lead to substantial variability and non-uniformity in the ON current [23]. In addition, a CNT network is comprised of individual single-walled CNTs (SWCNTs) of varying lengths ($L_t$) and alignment ($\theta$) with respect to the source and drain electrodes. Previous studies have shown that the variability in the CNT network morphology can significantly affect the channel resistance and device performance [24, 25]. Therefore these variations in the channel geometry and network morphology are very likely to influence the reliability and breakdown behavior of CN-TFTs as well. The variation in the breakdown behavior for a given TFT geometry can lead to instability and/or unreliability during the operation of CN-TFTs. Thus, it is very important to understand how the geometrical parameters affect the high-field operation of the CN-TFT in order to optimize the device design for reliable and uniform behavior. While our previous work [26] has correlated the electronic properties of SWCNTs within a CN-TFT channel to the device thermal reliability, the effects of channel geometry and network morphology on CN-TFT power and reliability have not been studied in detail.

In this work, we apply both experimental and computational methods to understand the breakdown behavior and thermal reliability of CN-TFTs. We examine the breakdown characteristics such as peak power (or breakdown power, $P_{BD}$) and the corresponding source-to-drain voltage referred to as the breakdown voltage ($V_{BD}$) of CN-TFTs in order to find their relation with the aforementioned geometrical parameters. We first analyze the breakdown characteristics and their standard deviations for smaller and larger $W_C$ at various $L_C$ for random networks with constant CNT length, $L_t$. Next, we systematically vary the alignment of CNTs in the network for a given $L_C$, $W_C$ and $L_t$ to study the effect of network alignment on the breakdown behavior. Subsequently, we consider a general case employing different log-normal distributions of $L_t$ in conjunction with several alignment distributions for a given $L_C$ and $W_C$. The results suggest that when $W_C$ is greater than the average $L_t$, $V_{BD}$ remains independent of $W_C$ and varies linearly with $L_C$. The variation in the distribution of alignment and $L_t$ does not significantly affect $V_{BD}$. However, we find that $P_{BD}$ increases with both $L_C$ and $W_C$. In particular, for large $W_C$, $P_{BD}$ varies linearly with both $W_C$ and $L_C$. Our results suggest that the thermal reliability of CN-TFTs can be improved by optimizing the CNT length and alignment distribution. The analysis presented here, provides new insight into optimizing the device parameters in order to engineer thermal reliability and uniformity in CN-TFT performance characteristics.

## 2. Methodology

Carbon nanotubes synthesized by arc discharge method are used as starting materials for all the samples. The diluted solution containing SWCNTs and surfactant is vacuum filtered through a mixed cellulose ester membrane to form CNT network followed by rinsing with water to remove the residual surfactant. The network is then transferred to supporting substrates of $SiO_2$ ($t_{ox}$ = 300 nm) on highly $n$-doped Si wafers ($t_{Si}$ = 500 μm) with predefined electrical contacts and then the filter is dissolved [26]. The device channels are patterned by photolithography and/or electron beam lithography (for submicron width dimensions). The Si substrate acts as a back-gate, and unless otherwise noted we set the gate-to-source voltage ($V_{GS}$ = -40 V) such that both $M$ and $S$ type CNTs in the network are in the "on" state ($V_{GS}$ is significantly below the threshold voltage) while the source-to-drain voltage ($V_{SD}$) is increased until network breakdown. Device characterization and breakdown were conducted in air at room temperature ambient ($T_0$ = 25 °C).

For computational analysis, we employ a coupled electro-thermal model to analyze the current, power, and temperature distribution in the device [21, 22, 27, 28]. A brief description about the governing equations is provided below.

### *2.1 Thermal Transport*

The thermal transport in the device consisting of CNT-network, oxide layer and Si substrate is simulated using the diffusive energy transport equations, which can be written in the following non-dimensional form [28]:

$$\frac{d^2\xi_i}{ds^{*2}} + \tilde{G}_S\left(\xi_{\mathrm{OX}} - \xi_i\right) + \sum_{\substack{\text{intersecting}\\ \text{tubes j}}} \tilde{G}_C\left(\xi_j - \xi_i\right) + \frac{d}{L_t}\frac{q_i^{'}}{Q^{'}} = 0 \qquad (1)$$

$$\nabla^{*2}\xi_{\mathrm{OX}} + \sum_{i=1}^{N_{tubes}} \tilde{G}_S\gamma\left(\xi_i - \xi_{\mathrm{OX}}\right) = 0 \qquad (2)$$

$$\nabla^{*2}\xi_{\mathrm{Si}} = 0 \qquad (3)$$

Here, $\xi = (T\text{-}T_\infty)/(Q^{'}dL_t/k_t)$ is the non-dimensional form of temperature ($T$). $T_\infty$ denotes the ambient temperature, $Q^{'}$ is a reference power per unit volume, $d$ is the diameter of CNT, and $k_t$ is the axial thermal conductivity of CNT. $\xi_i$, $\xi_{\mathrm{OX}}$ and $\xi_{\mathrm{Si}}$ are the non-dimensionalized temperatures of a section of the $i^{th}$ CNT, oxide, and Si, respectively. Asterisk symbol is used to refer to length variables which are non-dimensionalized by $d$. Equation (1) governs the temperature of any $i^{\mathrm{th}}$ CNT along its axial direction (length variable s); the second and third terms in this equation represent thermal interactions at CNT-oxide interface and at CNT-CNT junctions, respectively. $q_i^{'}$ is the volumetric Joule heating term within the CNT which is obtained from the solution of electrical transport equations (discussed below). $\tilde{G}_C$ and $\tilde{G}_S$ represent the non-dimensional thermal contact conductance at CNT-CNT junctions and CNT-oxide interface respectively and their estimated values are obtained from our previous work [21]. Equation (2) describes the temperature in the oxide layer and the second term in this equation represents CNT-oxide thermal interaction, which is summed over all the CNTs. The parameter $\gamma$ in this term characterizes the contact geometry. Equation (3) describes the temperature of the Si layer.

We use a constant temperature boundary condition ($T$ = 298 K) at the bottom surface of Si substrate, while a convective boundary condition [21, 28] is imposed at the top surface of the oxide layer. The lateral boundaries have been assumed to be thermally insulated. The boundary conditions have been selected to simulate the experimental conditions.

### 2.2 Electrical Transport

The electrical transport in the carbon nanotubes has been described by Poisson and current continuity equations as follows [13, 22, 28]:

$$\frac{d^2\psi_i}{ds^2} + \frac{\rho_i}{\varepsilon} - \frac{(\psi_i - V_G)}{\lambda^2} + \sum_{j\neq i}\frac{(\psi_j - \psi_i)}{\lambda_{ij}^2} = 0, \qquad (4)$$

$$\nabla . J_{pi} + \sum_{j\neq i} C_{ij}^{p}(p_j - p_i) = 0, \qquad (5)$$

$$\nabla . J_{ni} + \sum_{j\neq i} C_{ij}^{n}(n_j - n_i) = 0, \qquad (6)$$

Here, $\psi$ is the electrostatic potential, $V_G$ is the gate voltage, $\rho$ is the net charge density, $\varepsilon$ is the permittivity of CNT. The third term in Poisson equation represents the gating effect [28] with screening length, $\lambda = (\varepsilon_{CNT}\, t_{OX}\, d/\varepsilon_{OX})^{0.5}$. Here, $\varepsilon_{CNT}$ and $\varepsilon_{OX}$ are the dielectric constants for the CNT and gate oxide respectively and $t_{OX}$ is the oxide thickness. The forth term in Equation (4) describes the inter-tube electrostatic interaction at CNT-CNT junctions with screening length, $\lambda \sim d$. Equations (5) and (6) are current continuity equations for holes and electrons respectively, where $J$ is current density given by drift –diffusion equations. Hole and electron charge density are represented by $p$ and $n$,

respectively. The second term, $C_{ij}^{n}(n_j - n_i)$ or $C_{ij}^{p}(p_j - p_i)$, in the continuity equations represents charge (electrons or holes) transfer across the CNT-CNT junctions. The charge transfer coefficient ($C_{ij}^{n,p}$) is considered zero for *M*-*S* junctions to account for very low contact conductance compared to the *M*-*M* and *S*-S junctions [29]. The numerical values of major parameters in Equations (1-6) are provided in a separate table in the supplementary document. These electro-thermal equations are solved self-consistently to obtain the current, potential and temperature distribution in the CN-TFTs. Heterogeneous networks of *M* and *S* type CNTs (1:2 ratio) are considered in all simulations unless specified otherwise.

The model provides comprehensive details of the temperature and power distribution within the CNT network and thermal transport across substrate (Si) and insulator ($SiO_2$). Since these details are very difficult to obtain directly from the experiments, the model serves as an essential tool in analyzing the high-field transport and breakdown of CN-TFTs. The numerical model is validated by comparing the simulation results with the experimental data (see Section 3.1).

Under high field conditions, Joule heating can lead to oxidation of the CNTs in air if the temperature exceeds the breakdown temperature $T_{BD} \approx 600$ °C, resulting in the breakdown of the devices [20, 21, 30]. Thus, during this electrical breakdown process, the power dissipation in the device reaches a maximum value near $T_{BD}$, and then drops quickly to zero as the current paths within the network reform and oxidize, reaching catastrophic device failure. Back-gated device configuration has been selected for the experiments as it facilitates experimental measurements [20, 26]. All simulation results presented in this work are averaged over a large number of devices ($n \approx 100$) unless specified otherwise. Both mean as well as standard deviation of the breakdown characteristics are presented to understand the variability in the breakdown behavior for different device geometry and network morphology parameters.

## 3. Results and Discussion

### *3.1 Channel Geometry*

We first analyze the effect of $L_C$ and $W_C$ on the breakdown characteristics. From the perspective of the device breakdown, the two important metrics are $P_{BD}$ and $V_{BD}$. Fig. 2(a) shows the power dissipation in the device as a function of $V_{SD}$ for three different cases of $L_C$ = 5, 10, 15 μm at a network density of $\rho$ = 15 CNTs/μm$^2$, $W_C$ = 100 μm, and $L_t$ = 2 μm. We find an excellent match between the experimental and simulation results. It should be noted that smaller $L_C$ results in less resistance CNT networks which in turn leads to higher current (*i.e.*, higher power dissipation) at a given $V_{SD}$. This causes the device of smaller $L_C$ to break earlier (*i.e.*, at a lower $V_{SD}$). $V_{BD}$ and $P_{BD}$ both linearly scale with $L_C$ [Fig. 2(b) and 2(c)]. The error bars in these figures indicate the variation in breakdown characteristic of the random networks. The size of the error bar represents a 95 percent confidence interval for $V_{BD}$ (or $P_{BD}$). The experimental values for both $V_{BD}$ and $P_{BD}$ fall well within the range of error bars estimated from the simulations. For a given network density, the number of percolating pathways decreases as $L_C$ increases. As previously reported, [23] ON current shows greater variations when network density is decreased. Lowering the density is equivalent to reducing the number of percolating pathways, which also occurs when $L_C$ is increased, and therefore the error bars increase as $L_C$ increases. These results suggest that the variability in the breakdown for a given device geometry and network density can be substantial and require due consideration while predicting the device reliability [26].

Figure 3(a) shows the breakdown behavior of CN-TFTs for $W_C$ = 4, 10, 20, 30, and 40 μm at $L_C$ = 10 μm, $L_t$ = 2 μm and $\rho$ = 15 CNTs/μm$^2$. The curves in Fig. 3(a) resemble a 'bell' shape due to the statistical averaging. It can be observed that the $V_{BD}$ does not change with $W_C$. Further, we find $P_{BD}$ to be directly proportional to width when $W_C/L_t > 2$ [Fig. 3(b)]. We also note that the normalized standard deviation ($\sigma_{norm}$) of $V_{BD}$ [Fig. 3(c)] and $P_{BD}$ [Fig. 3(d)] increases when $L_C$ is increased or $W_C$ is decreased. For $W_C/L_t \leq 2$, we observe relatively large $\sigma_{norm}$ due to significant incremental change in the number of percolating pathways [31]. We find that for $\rho$ = 15 CNTs/μm$^2$, $L_C$ = 10 μm and $W_C/L_t$ = 2, less than 30% of the random networks out of 100 samples have a percolating path between source and drain. The probability of forming a percolating path further decreases as we increase $L_C$ for $W_C/L_t \leq 2$. Therefore, we employ a denser network to study the breakdown behavior for $W_C/L_t \leq 2$.

Figure 4 shows the dependence of breakdown behavior on $L_C$ for narrow width devices ($W_C/L_t$ = 0.75, 1, 1.5, 2) at $\rho$ = 30 CNTs/μm$^2$. We find that $V_{BD}$ is nearly invariant of the $W_C$ for $W_C/L_t \geq 1$ [Fig. 4(a)]. $P_{BD}$ follows width-dependent scaling with $L_C$ such that higher width leads to greater change in $P_{BD}$ per unit change in $L_C$ [Fig. 4(b)]. A similar trend is observed in the experiments as shown in the Supplementary Information (Section S1). We note that $\sigma_{norm}$ of $V_{BD}$ [Fig. 4(c)] and $P_{BD}$ [Fig. 4(d)] remain nearly invariant of $L_C$ for $W_C/L_t \geq 1$ and $\sigma_{norm}$ decreases as $W_C$ increases at a given $L_C$. Overall, we note that larger values of $L_C$ and $W_C$ correspond to better device reliability as they lead to larger $V_{BD}$, greater $P_{BD}$, and better uniformity in device characteristics.

Previous studies [20, 21, 26, 32] on the CN-TFT breakdown show that the network breaks along a zigzag pattern across the channel when $W_C$ is much greater than $L_t$. In the current study, we examine this breakdown pattern in CN-TFTs when $W_C$ is comparable to $L_t$. Scanning electron microscopy (SEM) images from the experiments show that the breakdown pattern remains zigzag when $L_C$ is small (few microns) for different values of $W_C$, as shown in Fig. 5 (a, d, g). Also, the length ($L_{BD}$) of the breakdown gap region [shown in Fig. 5(g)] is observed to be less than the average $L_t$ which indicates a highly localized burning of CNTs. Further, $L_{BD}$ increases as $L_C$ is increased for a given $W_C$ but does not change much with respect to $W_C$ for a given $L_C$ (Fig. 5). This trend underlines the role of temperature profile before the breakdown and electrostatic effects of the broken CNTs during the breakdown process. For devices with larger $L_C$, the temperature profile is more flat away from the contacts which leads to larger $L_{BD}$. In addition, higher electrostatic effect from the broken tubes amounts to greater induced electric field in the unbroken neighboring CNTs. This electrostatic effect is proportional to the applied voltage between source and drain at the breakdown (*i.e.,* $V_{BD}$) [32]. As $V_{BD}$ linearly increases with $L_C$, the breakdown gap also follows nearly the same trend.

### *3.2 Network Morphology*

#### 3.2.1 Variable alignment angle with constant CNT length

In order to investigate the effect of CNT alignment on TFT breakdown behavior, we consider several alignment distributions of CNTs in the network. We define average alignment ($\theta_{avg}$) such that for a specific value of $\theta_{avg}$, a CNT in the network is allowed to make any angle between $-2\theta_{avg}$ and $2\theta_{avg}$ with equal probability, as shown in Fig. 6.

Figure 7(a) shows a plot of power dissipation versus $V_{SD}$ for different network alignments (from $\theta_{avg}$ = 9°- 45°). It is observed that for a highly aligned network ($\theta_{avg}$ < 10°), devices show negligible current due to the reduced number of percolating pathways bridging the source and drain contacts. However, as we increase $\theta_{avg}$, the current increases due to the increasing number of percolating pathways. Previous studies [22] have also suggested that the ON current depends on the alignment and it reaches a maximum at $\theta_{avg} \sim 30°$ which is consistent with our results for $V_{SD}$ < 20 V, as shown in Fig. 7(a). For the breakdown behavior analysis, we analyze $P_{BD}$ and $V_{BD}$ dependence on $\theta_{avg}$. We find that the $V_{BD}$ first decreases sharply and then shows a zigzag pattern with increasing $\theta_{avg}$. Two local minima are observed at $\theta_{avg}$ = 22° and $\theta_{avg}$ = 36° [Fig. 7(b)]. $V_{BD}$ lies in the small range of 26 V to 29 V for $\theta_{avg}$ > 10° which suggests a weak dependence of $V_{BD}$ on alignment. The $P_{BD}$ increases linearly as we increase $\theta_{avg}$ up to 27° and two 'local' maxima are observed at $\theta_{avg}$ = 27° and $\theta_{avg}$ = 40° [Fig. 7(c)].

In order to explore the nature of this dependence, we examine the breakdown pattern of the CNT networks. It should be noted that we consider the network to be composed of *M* and *S* type CNTs in 1:2 ratio. A Schottky barrier has been assumed to be present between metallic and semiconducting CNTs, and *M*-*S* junctions are considered to be electrically insulating since *M*-*M* or *S*-*S* junction conductance can be 2 orders of magnitude higher than *M*-*S* junction conductance [29]. We also showed in our previous work [21] that in general heat transfer across the CNT junctions is negligible in comparison to heat transfer across CNT-$SiO_2$ interface. Therefore the poor thermal contact conductance between CNTs makes crossed-CNT contacts thermally insulating as well [21]. This implies that the network can be considered to be composed of two independent 'parallel' networks of different densities and conductivities. Therefore the breakdown behavior and characteristics discussed are due to the combined breakdown behavior of pure metallic and semiconducting networks. Figure 8(a) shows a plot of power dissipation versus $V_{SD}$ for different $\theta_{avg}$ at $\rho$ = 15 CNTs/μm$^2$ of a homogeneous network (semiconducting CNTs only). We find that $V_{BD}$ and $P_{BD}$ exhibit only one minima ($\theta_{avg}$ = 20°) and maxima ($\theta_{avg}$ = 36°) respectively [Fig. 8(b) and (c)]. A similar trend is observed for pure metallic CNT networks. It should be noted, however, that the density of the metallic and semiconducting networks is in a 1:2 ratio within the combined network, and the location of maxima or minima of the breakdown characteristics depends on $\rho$ [Fig. 9(a) and (b)]. This is responsible for the existence of the two local optimum points in breakdown characteristics of the heterogeneous network.

### 3.2.2 Variable alignment angle with lognormal distribution of CNT length

We previously discussed the dependence of breakdown behavior on alignment of CNTs where $L_t$ was kept constant. In this section, we study the breakdown behavior for a more general case where both CNT length and alignment are varied according to their respective distributions. Figure 10 illustrates the log normal distribution of $L_t$ in the network. Here, the device size is $L_C \times W_C = 5 \times 5$ μm, and $\rho = 15$ CNTs/μm$^2$. All CNTs are considered to be semiconducting to analyze only the effects of length and alignment distributions. We consider three different cases of log-normal length distributions (average $L_t$, $\langle L_t \rangle = 1$ μm, 1.15 μm and 1.3 μm) and 9 cases of alignment distributions (range of $\theta_{avg} = 9°$ (highly aligned network) to 45° (random network)). The log-normal distribution is given by following equation:

$$f(L_t, \mu, \sigma) = \frac{1}{L_t \sigma \sqrt{2\pi}} \exp\left[ -\frac{(\ln L_t - \mu)^2}{2\sigma^2} \right] \tag{7}$$

where $f$ is the probability distribution function, $L_t$ is the CNT length, $\mu$ is the mean and $\sigma$ is the standard deviation of the CNT length. It should be noted that the lognormal distribution of CNT length has a practical significance as this distribution is typically observed in the experiments [26, 33]. We expect the log-normal distribution to affect the reliability and breakdown characteristics of homogenous CNT networks, as a previous study [25] reported that the resistivity of heterogeneous networks varies with the change in the parameters of the log-normal distribution.

Results (Fig. 11) suggest that the effect of the alignment on the breakdown behavior strongly depends on $L_t$ distribution. We find that a $L_t$ distribution with higher $\langle L_t \rangle$ provides higher $P_{BD}$. Also, the $\theta_{avg}$ corresponding to the maximum $P_{BD}$ decreases when $\langle L_t \rangle$ is increased. In other words, better thermal reliability can be obtained when $\langle L_t \rangle$ is higher and the network is partially aligned. Interestingly, $V_{BD}$ does not show much variation despite the fact that $P_{BD}$ changes significantly. The trend of $P_{BD}$ can be explained on the basis of the trade-off associated with the number of percolating paths and resistance of these paths. At lower $\theta_{avg}$, the number of percolating paths in the channel will be less, but the resistance of these pathways will be also low due to the lower number of CNT junctions in these pathways. For higher values of $\theta_{avg}$, the network tends toward a random distribution and the number of connections in the network increases, i.e., the number of effective percolative pathways increases, but the CNT junction density per pathway also increases. Therefore a maximum current (or power) should be achieved for some intermediate $\theta_{avg}$ which offers optimal channel resistance. As mentioned earlier, this optimal value of $\theta_{avg}$ decreases as $\langle L_t \rangle$ increases. We also note that the standard deviation in $V_{BD}$ and $P_{BD}$ shows little variation with change in $\langle L_t \rangle$ and $\theta_{avg}$. However, the normalized value of it ($\sigma_{norm}$) changes due to the variation in the mean values of the respective variables [Fig. 12(a) and (b)]. More details about power variation with $V_{SD}$ have been included in the Supplementary Information (Section S2).

## 4. Conclusion

In summary, we have studied the effects of channel geometry and network morphology on the high field breakdown of carbon nanotube network thin film transistors (CN-TFTs). We apply both experimental and computational techniques to examine the heat dissipation in the device and provide an in-depth analysis of two important characteristics ($P_{BD}$ and $V_{BD}$) relevant to the breakdown process in CN-TFTs. We observe that the breakdown characteristics vary significantly with the channel length, but their dependence on the channel width is relatively very small. In a heterogeneous network, the breakdown characteristics and their relation with the network morphology vary with the ratio of metallic and semiconducting CNTs in the network. The analysis on breakdown behavior of CN-TFT for various log-normal CNT length distribution and several alignment distributions suggests that the heat dissipation and thermal reliability of CN-TFTs can be significantly improved by optimizing the network morphology parameters.

**Acknowledgement**

Work at the University of Illinois Urbana-Champaign was sponsored in part by the National Science Foundation (NSF) CAREER grant ECCS 0954423 (E.P.), the NSF Graduate Research Fellowship (D.E.), and the Office of Naval Research (ONR) grant N00014-10-1-0853 (A.B.). M.P.G. acknowledges support from NSF grant ECCS-1028569. The authors thank Mark C. Hersam, Vinod Sangwan and Deep Jariwala for providing CNT networks and Edmond Chow for electron-beam (e-beam) lithography.

**Supplementary Material**

Supplementary material (additional results related to experimental breakdown characteristics and power-voltage curves for lognormal CNT length distributions) is available in the online version of this article.

**References**

[1] Reuss R H, Chalamala B R, Moussessian A, Kane M G, Kumar A, Zhang D C, Rogers J A, Hatalis M, Temple D, Moddel G, Eliasson B J, Estes M J, Kunze J, Handy E S, Harmon E S, Salzman D B, Woodall J M, Alam M A, Murthy J Y, Jacobsen S C, Olivier M, Markus D, Campbell P M and Snow E 2005 Macroelectronics: Perspectives on Technology and Applications *Proc. IEEE* **93** 1239-56

[2] Cao Q and Rogers J A 2009 Ultrathin Films of Single-Walled Carbon Nanotubes for Electronics and Sensors: A Review of Fundamental and Applied Aspects *Adv. Mater.* **21** 29-53

[3] Ha M, Xia Y, Green A A, Zhang W, Renn M J, Kim C H, Hersam M C and Frisbie C D 2010 Printed, Sub-3V Digital Circuits on Plastic from Aqueous Carbon Nanotube Inks *ACS Nano* **4** 4388-95

[4] Hu L, Hecht D S and Grüner G 2010 Carbon Nanotube Thin Films: Fabrication, Properties, and Applications *Chem. Rev.* **110** 5790-844

[5] Kocabas C, Pimparkar N, Yesilyurt O, Kang S J, Alam M A and Rogers J A 2007 Experimental and Theoretical Studies of Transport through Large Scale, Partially Aligned Arrays of Single-Walled Carbon Nanotubes in Thin Film Type Transistors *Nano Lett.* **7** 1195-202

[6] Schymura S, Kühnast M, Lutz V, Jagiella S, Dettlaff-Weglikowska U, Roth S, Giesselmann F, Tschierske C, Scalia G and Lagerwall J 2010 Towards Efficient Dispersion of Carbon Nanotubes in Thermotropic Liquid Crystals *Adv. Funct. Mater.* **20** 3350-7

[7] Wang C, Takei K, Takahashi T and Javey A 2013 Carbon nanotube electronics - moving forward *Chem. Soc. Rev.* **42** 2592-609

[8] Park S, Vosguerichian M and Bao Z 2013 A review of fabrication and applications of carbon nanotube film-based flexible electronics *Nanoscale* **5** 1727-52

[9] Okuda S, Okamoto S, Ohno Y, Maehashi K, Inoue K and Matsumoto K 2012 Horizontally Aligned Carbon Nanotubes on a Quartz Substrate for Chemical and Biological Sensing *J. Phys. Chem. C* **116** 19490-5

[10] Alizadegan R, Liao A, Xiong F, Pop E and Hsia K 2012 Effects of tip-nanotube interactions on atomic force microscopy imaging of carbon nanotubes *Nano Res.* **5** 235-47

[11] Sun D-m, Timmermans M Y, Tian Y, Nasibulin A G, Kauppinen E I, Kishimoto S, Mizutani T and Ohno Y 2011 Flexible high-performance carbon nanotube integrated circuits *Nat. Nano.* **6** 6

[12] Kumar S, Murthy J Y and Alam M A 2005 Percolating Conduction in Finite Nanotube Networks *Phys. Rev. Lett.* **95** 066802

[13] Kumar S, Pimparkar N, Murthy J Y and Alam M A 2006 Theory of transfer characteristics of nanotube network transistors *Appl. Phys. Lett.* **88** 123505

[14] Cao Q, Hur S H, Zhu Z T, Sun Y G, Wang C J, Meitl M A, Shim M and Rogers J A 2006 Highly Bendable, Transparent Thin-Film Transistors That Use Carbon-Nanotube-Based Conductors and Semiconductors with Elastomeric Dielectrics *Adv. Mater.* **18** 304-9

[15] Cao Q, Kim H-s, Pimparkar N, Kulkarni J P, Wang C, Shim M, Roy K, Alam M A and Rogers J A 2008 Medium-scale carbon nanotube thin-film integrated circuits on flexible plastic substrates *Nature* **454** 495-500

[16] Wang C, Zhang J, Ryu K, Badmaev A, De Arco L G and Zhou C 2009 Wafer-Scale Fabrication of Separated Carbon Nanotube Thin-Film Transistors for Display Applications *Nano Lett.* **9** 4285-91

[17] Arnold M S, Green A A, Hulvat J F, Stupp S I and Hersam M C 2006 Sorting carbon nanotubes by electronic structure using density differentiation *Nat. Nano.* **1** 6

[18] Cao Q, Han S-j, Tulevski G S, Zhu Y, Lu D D and Haensch W 2013 Arrays of single-walled carbon nanotubes with full surface coverage for high-performance electronics *Nat. Nano.* **8** 180-6

[19] Sun D-m, Timmermans M Y, Tian Y, Nasibulin A G, Kauppinen E I, Kishimoto S, Mizutani T and Ohno Y 2011 Flexible high-performance carbon nanotube integrated circuits *Nat. Nano.* **6** 156-61

[20] Estrada D and Pop E 2011 Imaging Dissipation and Hot Spots in Carbon Nanotube Network Transistors *Appl. Phys. Lett.* **98** 073102

[21] Gupta M P, Chen L, Estrada D, Behnam A, Pop E and Kumar S 2012 Impact of thermal boundary conductances on power dissipation and electrical breakdown of carbon nanotube network transistors *J. Appl. Phys.* **112** 124506

[22] Pimparkar N, Cao Q, Kumar S, Murthy J Y, Rogers J and Alam M A 2007 Current and Voltage Characteristics of Long-Channel Nanobundle Thin-Film Transistors: "Bottom-Up" Perspective *IEEE Electron Device Lett.* **28** 157-60

[23] Pimparkar N, Cao Q, Rogers J and Alam M 2009 Theory and practice of "Striping" for improved ON/OFF Ratio in carbon nanonet thin film transistors *Nano Res.* **2** 167-75

[24] Timmermans M, Estrada D, Nasibulin A, Wood J, Behnam A, Sun D-m, Ohno Y, Lyding J, Hassanien A, Pop E and Kauppinen E 2012 Effect of carbon nanotube network morphology on thin film transistor performance *Nano Res.* **5** 307-19

[25] Hicks J, Behnam A and Ural A 2009 Resistivity in percolation networks of one-dimensional elements with a length distribution *Phys. Rev. E* **79** 012102

[26] Behnam A, Sangwan V K, Zhong X, Lian F, Estrada D, Jariwala D, Hoag A J, Lauhon L J, Marks T J, Hersam M C and Pop E 2013 High-Field Transport and Thermal Reliability of Sorted Carbon Nanotube Network Devices *ACS Nano* **7** 482

[27] Kumar S, Alam M A and Murthy J Y 2007 Computational Model for Transport in Nanotube-Based Composites With Applications to Flexible Electronics *J. Heat Transfer* **129** 500-8

[28] Kumar S, Pimparkar N, Murthy J Y and Alam M A 2011 Self-Consistent Electrothermal Analysis of Nanotube Network Transistors *J. Appl. Phys.* **109** 014315

[29] Fuhrer M S, Nygård J, Shih L, Forero M, Yoon Y-G, Mazzoni M S C, Choi H J, Ihm J, Louie S G, Zettl A and McEuen P L 2000 Crossed Nanotube Junctions *Science* **288** 494-7

[30] Hata K, Futaba D N, Mizuno K, Namai T, Yumura M and Iijima S 2004 Water-Assisted Highly Efficient Synthesis of Impurity-Free Single-Walled Carbon Nanotubes *Science* **306** 1362-4

[31] Li J and Zhang S-L 2009 Finite-size scaling in stick percolation *Phys. Rev. E* **80** 040104

[32] Shekhar S, Erementchouk M, Leuenberger M N and Khondaker S I 2011 Correlated electrical breakdown in arrays of high density aligned carbon nanotubes *Appl. Phys. Lett.* **98** 243121

[33] Sangwan V K, Ortiz R P, Alaboson J M P, Emery J D, Bedzyk M J, Lauhon L J, Marks T J and Hersam M C 2012 Fundamental Performance Limits of Carbon Nanotube Thin-Film Transistors Achieved Using Hybrid Molecular Dielectrics *ACS Nano* **6** 7480-8

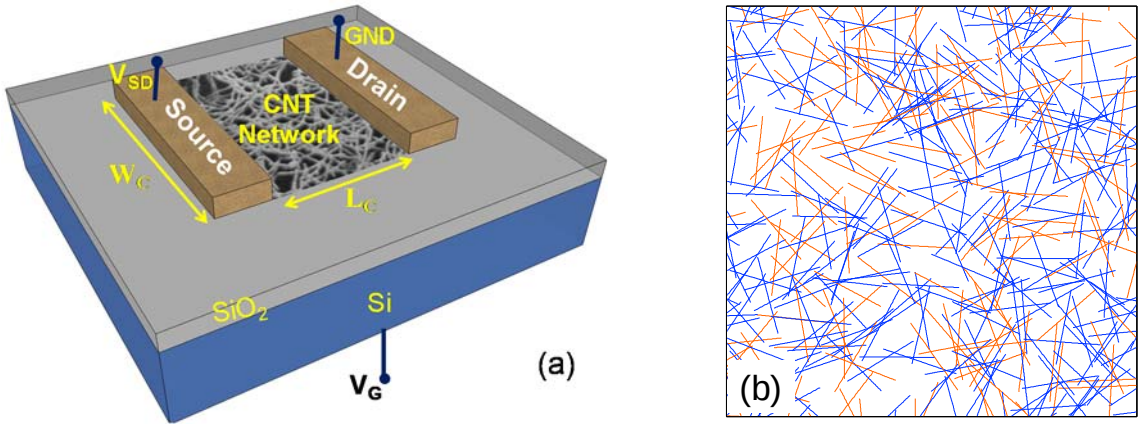


**Figure 1.** Schematic of (a) back-gated CN-TFT device with channel length (*Lc*) and channel width ($W_C$) similar to the devices experimentally tested. (b) A sample of simulated random network of CNTs; blue color is used for semiconducting and red for metallic CNTs.

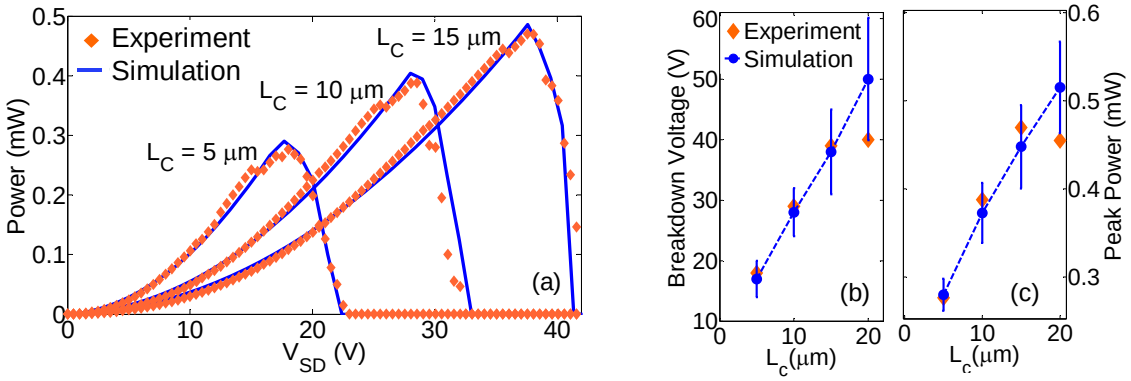


**Figure 2.** (a) Measured and simulated power dissipation in a CNT network versus source-to-drain voltage ($V_{SD}$) for three different channel lengths ($L_C$ = 5, 10, 15 μm). Simulation results are presented for individual devices here. For a given $L_C$, power reaches a peak value and then drops quickly to zero as the CNT network breaks down due to the excessive Joule heating and CNT oxidation in air. The value of $V_{SD}$ corresponding to the peak power ($P_{BD}$) is referred to as the breakdown voltage, $V_{BD}$. (b) $V_{BD}$ versus $L_C$, and (c) $P_{BD}$ versus $L_C$. The error bar represents a 95 percent confidence interval. The device is in the ON state at gate voltage $V_{GS}$ = -40V. Device width $W_C$ = 100 μm; CNT length $L_t$ = 2 μm, network density $\rho$ = 15 CNTs/μm$^2$. (b) and (c) contain simulation results which are averaged over 100 devices.

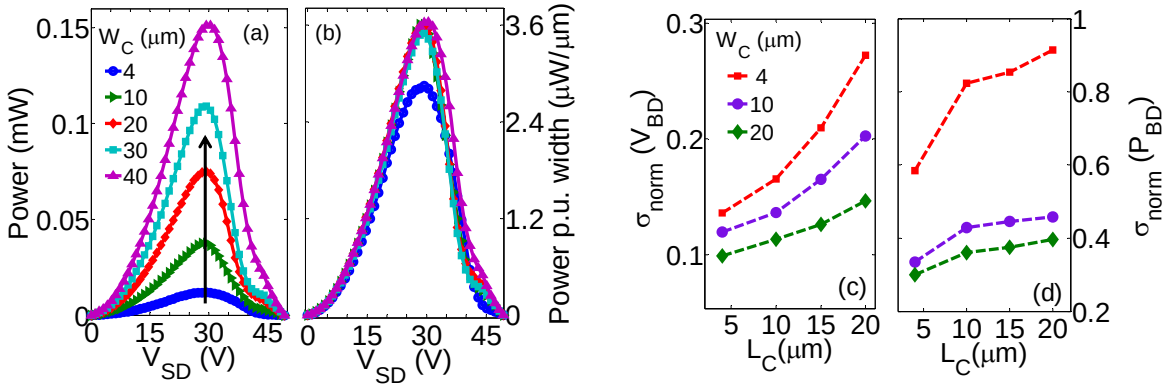


**Figure 3.** Numerical results for (a) power vs. $V_{SD}$ (arrow indicates the increasing channel width), (b) power per unit width vs. $V_{SD}$ for several channel widths ($W_C$ = 4, 10, 20, 30, 40 μm); channel length, $L_C$ = 10 μm, and network density, $\rho$ = 30 CNTs/μm$^2$. Note that power per unit width becomes invariant with respect to $W_C$ for sufficiently high $W_C$. (c) $\sigma_{norm}$ of breakdown voltage ($V_{BD}$) vs. $L_C$, and (d) $\sigma_{norm}$ of peak power ($P_{BD}$) vs. $L_C$. Here $\sigma_{norm}$ = standard deviation / mean.

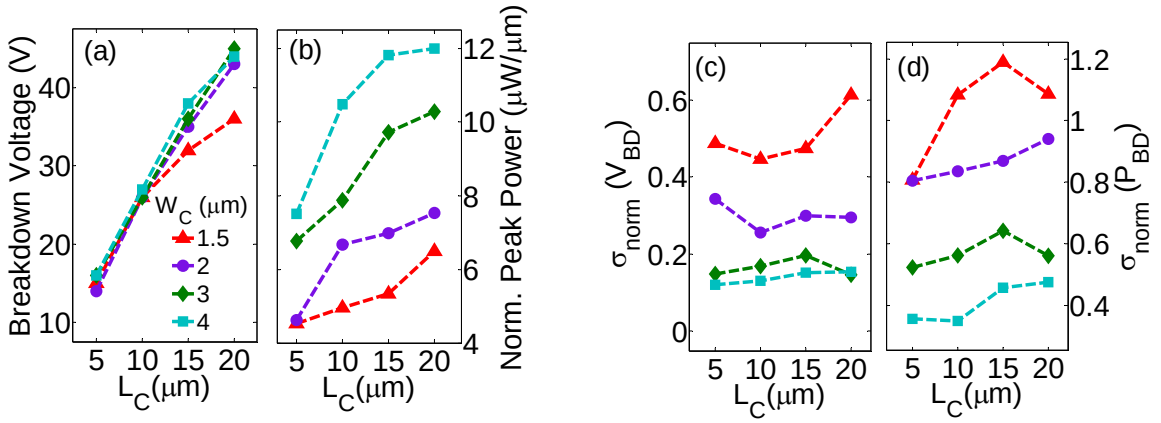


**Figure 4.** Numerical results for (a) breakdown voltage ($V_{BD}$) and (b) normalized peak power (with respect to $W_C$) in the CNT network vs. channel length ($L_C$) for smaller channel widths ($W_C$). (c) $\sigma_{norm}$ of $V_{BD}$, (d) Peak power ($PP$) vs. $L_C$. Here, network density $\rho$ = 30 CNTs/μm$^2$.

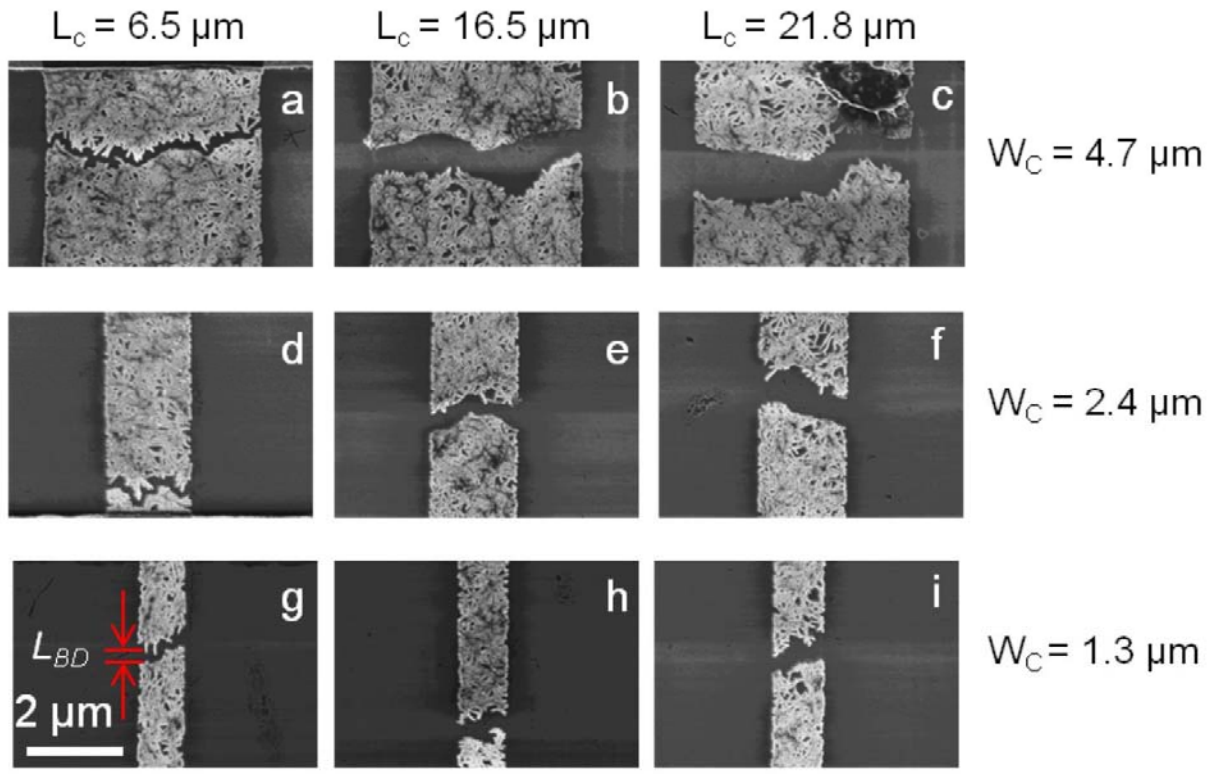


**Figure 5.** Scanning electron microscopy (SEM) images of CN-TFTs after complete breakdown for different channel lengths ($L_C$ = 6.5 µm, 16.5 µm, 21.8 µm) and widths ($W_C$ = 1.3 µm, 2.4 µm, 4.7 µm). The breakdown gap length ($L_{BD}$) in the CN-TFT increases as the $L_C$ is increased; however $L_{BD}$ does not show much variation when the width is changed.

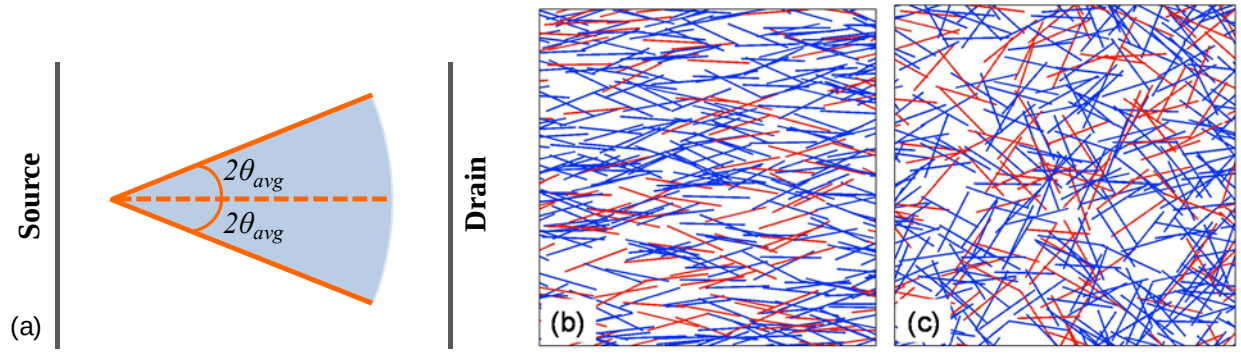


**Figure 6.** (a) The schematic illustrates the alignment of a CNT. The average alignment ($\theta_{avg}$) of the CNT network is defined such that for a specific value of $\theta_{avg}$, a CNT in the network is allowed to make any angle between -2$\theta_{avg}$ and 2$\theta_{avg}$ with equal probability. Hence, by this definition, $\theta_{avg}$ = 45° corresponds to a random network, and $\theta_{avg}$ = 0° means perfectly aligned CNTs. A example of heterogeneous CNT network with (b) $\theta_{avg}$ = 13°; (c) $\theta_{avg}$ = 36°. Metallic (M) CNTs in brown, semiconducting (S) CNTs in blue; M:S network density ratio is 1:2.

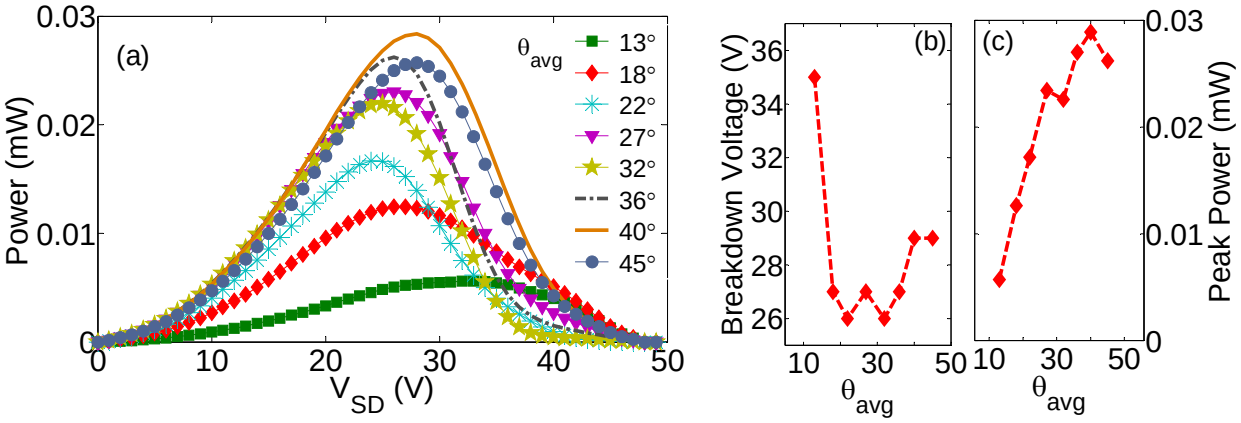


**Figure 7.** (a) Power dissipation vs. source-to-drain voltage ($V_{SD}$) for different alignments ($\theta_{avg}$) of CNTs in the network. (b, c) $V_{BD}$ and $P_{BD}$ vs. $\theta_{avg}$ respectively. Here, $L_t = 2$ µm, $L_C = 10$um, $W_C = 10$ µm, $\rho = 15$ CNTs/µm$^2$. Metallic to semiconducting CNT ratio in the network is 1:2 and their electrical conductivity ratio is 5:1. It should be noted that very few (< 10%) devices have connected pathways at very low angle ($\theta_{avg} < 10°$). However, this number improves (e.g. >70% for $\theta_{avg} = 13°$) significantly for higher $\theta_{avg}$.

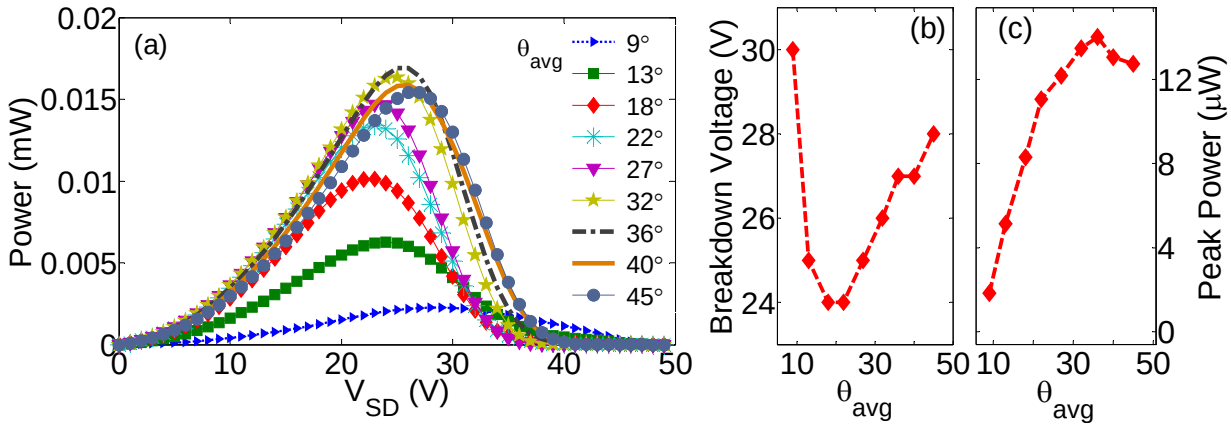


**Figure 8.** (a) Plot of power dissipation in the device vs. source-to-drain voltage ($V_{SD}$) for different alignments ($\theta_{avg}$) of CNTs of purely semiconducting network. (b), (c) breakdown voltage ($V_{BD}$) and peak power ($P_{BD}$) are plotted vs. $\theta_{avg}$. Here $L_t = 2$ µm, $L_C = 10$ µm, $W_C = 10$ µm, and $\rho = 15$ CNTs/µm$^2$.

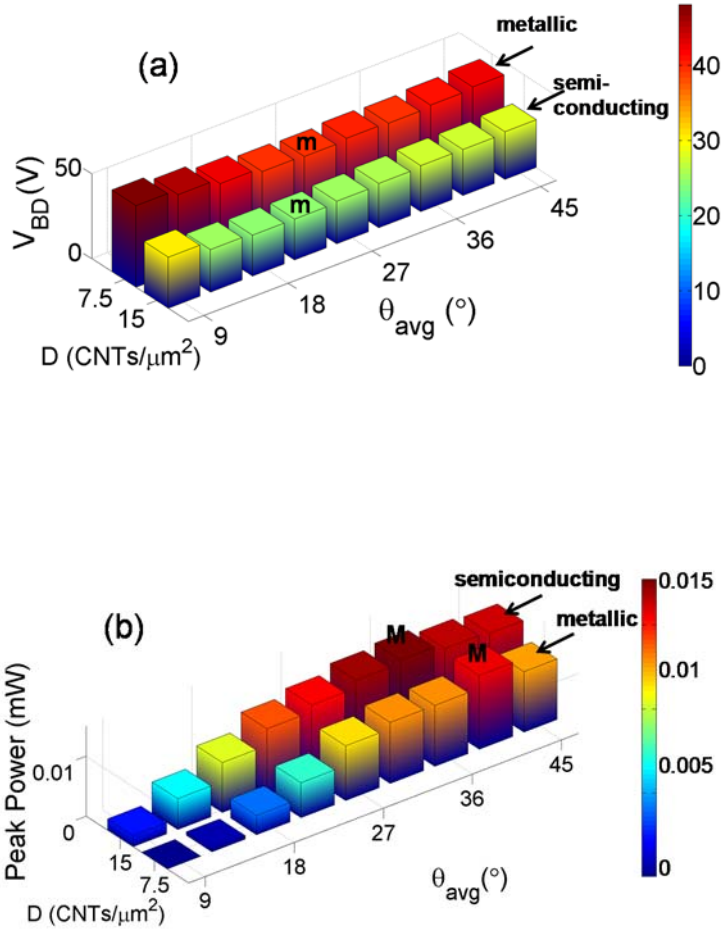


**Figure 9.** A bar plot of (a) breakdown voltage ($V_{BD}$), (b) peak power dissipation ($P_{BD}$) versus network alignment ($\theta_{avg}$) for metallic ($\rho$ = 7.5 CNTs/μm$^2$) and semiconducting ($\rho$ = 15 CNTs/μm$^2$) networks. Letters 'm' and 'M' denote the location of minima and maxima respectively. The metallic to semiconducting CNT density ratio is 1:2 which is same as that in typical unsorted CNT network.

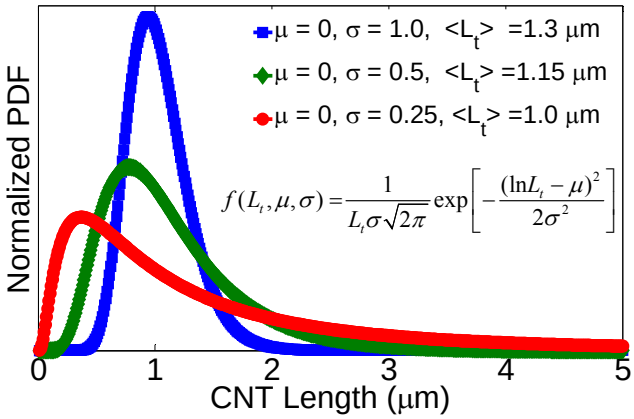


**Figure 10.** Three different log-normal CNT length distributions in the network with average CNT length, $<L_t>$ = 1 μm, 1.15 μm and 1.3 μm.

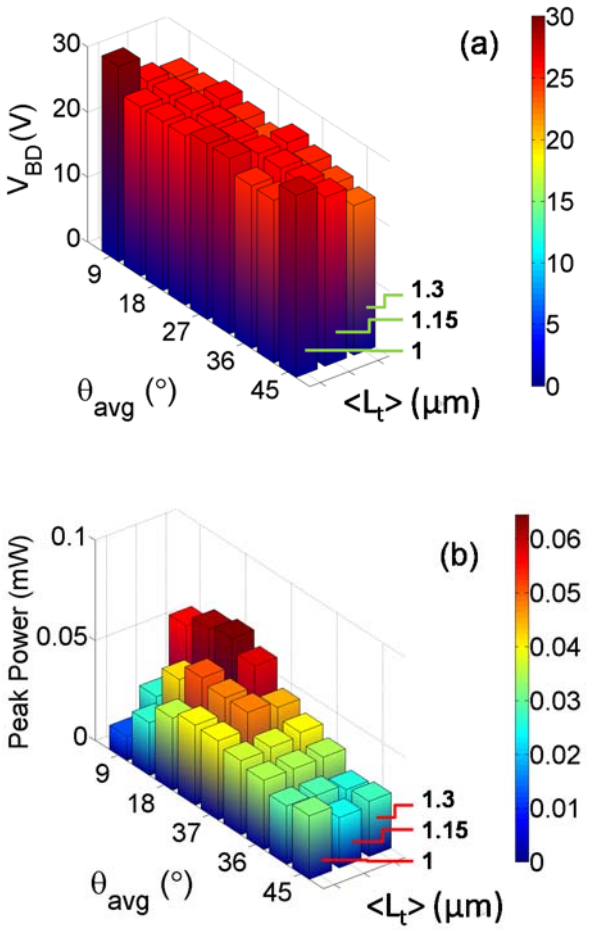


**Figure 11.** A bar plot of (a) breakdown voltage ($V_{BD}$) (b) peak power ($P_{BD}$) for different alignment and length distributions of the CNT network. The $V_{BD}$ shows little variation as alignment or length distribution is changed, whereas the $P_{BD}$ shows a strong correlation with alignment; this correlation changes significantly as length distribution is changed.

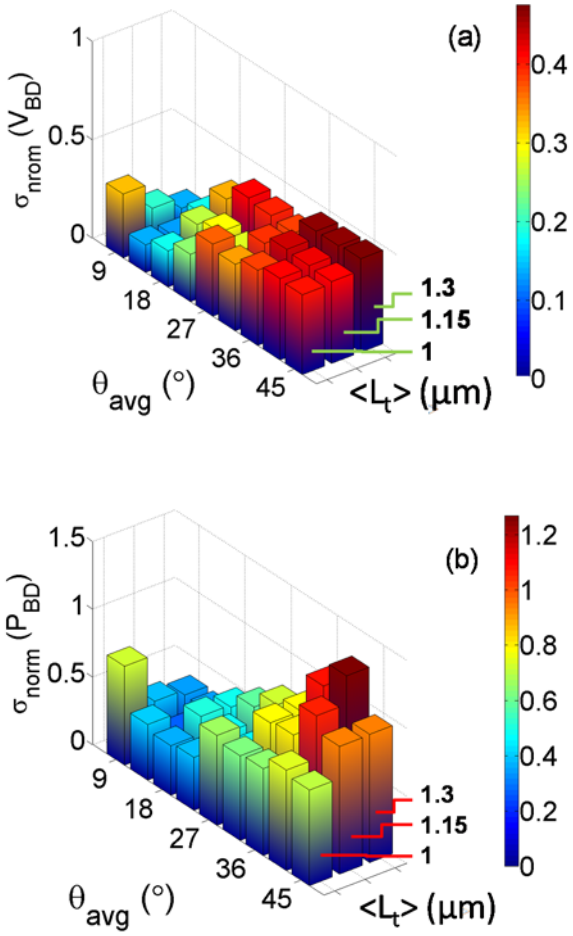


**Figure 12.** A bar plot of normalized standard deviation ($\sigma_{norm}$) of (a) breakdown voltage ($V_{BD}$), (b) peak power ($P_{BD}$) for different alignment and length distributions of the CNT network.

# Supporting Information

**Table of Parameters used in Electro-Thermal Model**

| Variable | Name | Nominal Value |
|---|---|---|
| $\xi = (T-T_\infty)/(Q^{'}dL_t/k_t)$ | Non-dimensional Temperature | - |
| $T$ | Temperature | (Kelvin) |
| $T_\infty$ | Ambient Temperature | 298 K |
| $d$ | Diameter | 2 nm |
| $L_t$ | CNT length | 2 μm |
| $k_t$ | Thermal conductivity of CNT | 1000 W/mK |
| $k_{OX}$ | Thermal conductivity of oxide | 1 W/mK |
| $t_{OX}$ | Oxide thickness | 300 nm |
| $t_{Si}$ | Si thickness | 500 μm |
| $\tilde{G}_S$ | Non-dimensional thermal conductance at CNT-oxide interface | $2 \times 10^{-4}$ |
| $\tilde{G}_C$ | Non-dimensional thermal conductance at CNT-CNT junction | $10^{-7}$ |
| $C_{ij}$ | Charge transfer coefficient | 50 |

**S1. Breakdown Characteristics from Experimental Results**

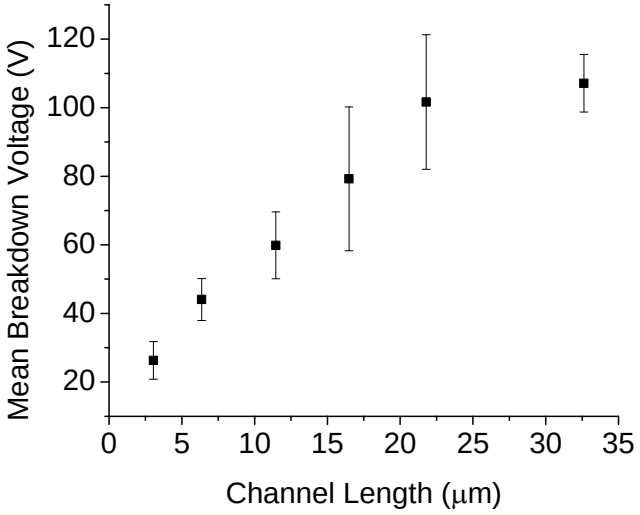


**Figure S-1** Variation of the breakdown voltage $V_{BD}$ versus channel length ($L_C$). Experimental results are obtained for limited number of devices (total ~30 devices including all the cases). Nevertheless, the general trend agrees well with the simulation results.

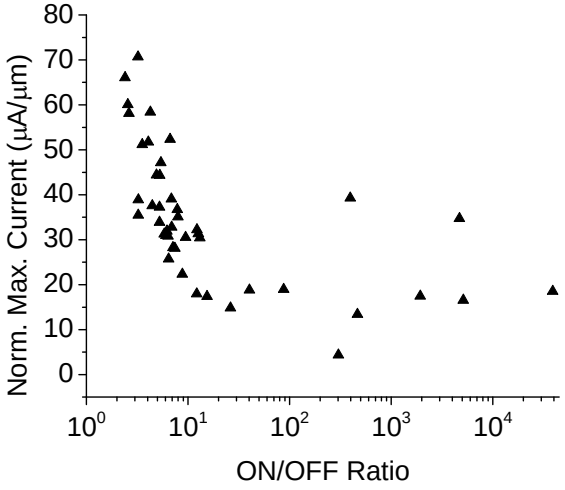


**Figure S-2** Variation of normalized maximum current (normalized with respect to $W$) versus ON/OFF ratio of CN-TFTs. For devices with higher ON/OFF ratio, the maximum current density before breakdown is observed to be lower compared to the devices with lower ON/OFF ratio. We observed that for semiconducting networks the maximum current is usually lower than the metallic network. Therefore, narrow networks which have more semiconducting paths show lower current capacity. It should be noted that such dependence is observed only when $W$ is less than or comparable to average CNT length and does not exist in case of larger $W$.

**S2. Breakdown Behavior for Different Orientation Distributions and Lognormal CNT Length Distributions**

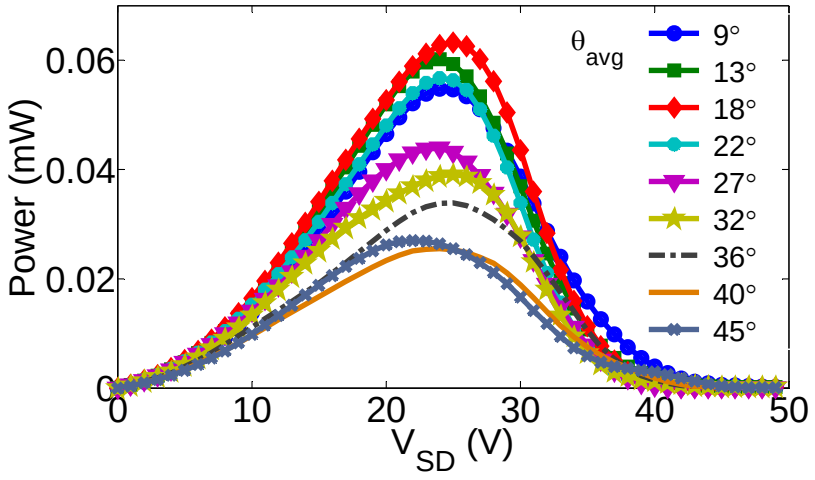


**Figure S-3**. Variation in power dissipation with source-to-drain voltage for several alignment cases; CNT length distribution corresponds to μ = 0, σ = 1 and average CNT length = 1.3 μm. Maximum power dissipation increases with $\theta_{avg}$ for $\theta_{avg}$ = 9° to 18°, however it decreases significantly for further increase in $\theta_{avg}$, i.e., the maximum power dissipation is highest for $\theta_{avg}$ = 18°. It can be noted that the random network ($\theta_{avg}$ = 45°) shows the poorest performance from the point of breakdown behavior and thermal reliability. Interestingly, the voltage corresponding to the peak power does not vary much as $\theta_{avg}$ is changed despite the fact that peak power can change upto three times in the range of $\theta_{avg}$ considered.

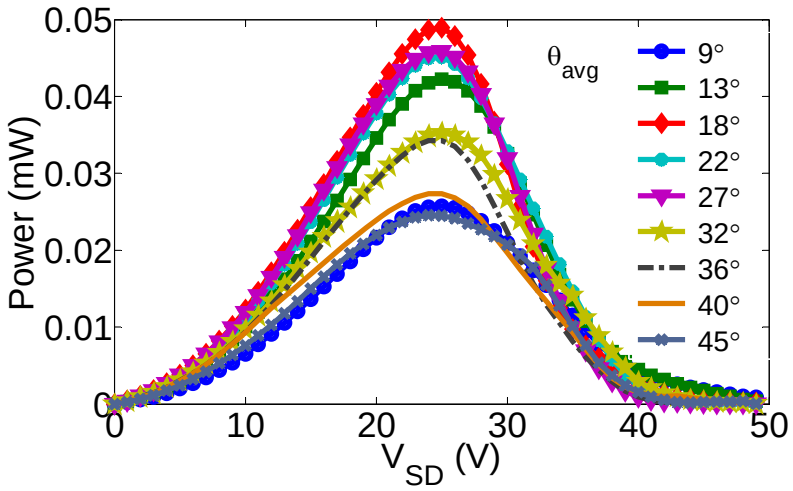


**Figure S-4**. Variation in power dissipation with source-to-drain voltage for several alignmentcases; CNT length distribution corresponds to μ = 0, σ = 0.5 and average CNT length = 1.15 μm. Maximum power dissipation is highest for $\theta_{avg}$ = 18°. It can be noted here that both highly aligned ($\theta_{avg}$ = 9°) and random network ($\theta_{avg}$ = 45°) show the poorest performance from the point of breakdown behavior and thermal reliability.

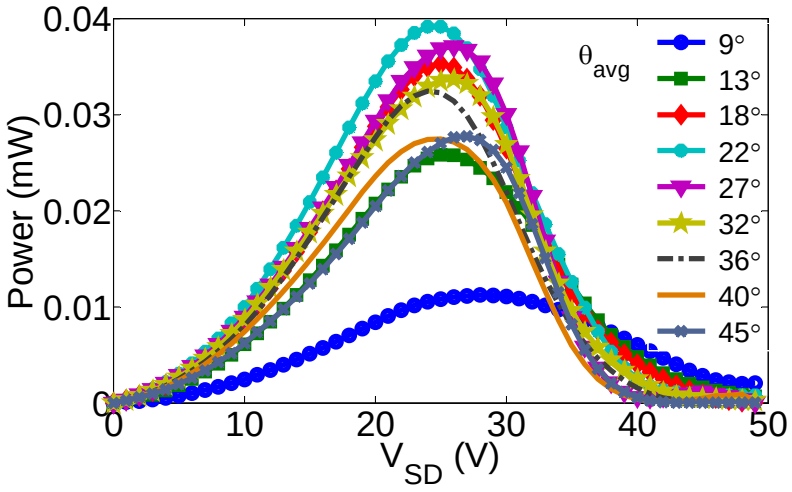


**Figure S-5**. Variation in power dissipation with source-to-drain voltage for several alignment cases; CNT length distribution corresponds to $\mu = 0$, $\sigma = 0.25$ and average CNT length = 1 μm. Maximum power dissipation is highest for $\theta_{avg} = 22°$. It can be noted here that the highly aligned network ($\theta_{avg} = 9°$) shows the poorest performance from the point of breakdown behavior and thermal reliability. Also, the difference in the highest maximum power dissipation (at $\theta_{avg} = 22°$) and maximum power dissipation of random network ($\theta_{avg} = 45°$) is significantly less compared to previous two cases (see Figs. S3 and S4). This trend is very similar to that obtained for constant CNT length case since the lognormal CNT length distribtion for this case closely resembles to constant CNT length case.